Electronic Structures and d–d Spectra of Vanadium(IV) and VO^{2+} Complexes: Discrete Variational Xα Calculations*

Robert J. Deeth
School of Chemistry, University of Bath, Claverton Down, Bath BA2 7AY, UK

Discrete Variational Xα(DVXα) calculations at three successive levels of approximation have been carried out for the vanadium(IV) complexes VCl_4, $[VCl_5]^-$, $[VOCl_4]^{2-}$, $[VO(NCS)_4]^{2-}$, $[VO(NCS)_4(OH_2)]^{2-}$, $[VO(CN)_5]^{3-}$, $[VO\{OC(NH_2)_2\}_2Cl_2]$ and $[VO(NMe_3)_2Cl_2]$. The electronic structures and the nature of the metal–ligand bonding are described and compared with previous theoretical results and a detailed comparison between observed and computed d–d electronic transition energies is presented. Near-quantitative agreement is obtained for the observed band maxima. The calculated assignments from the most accurate calculations are also in agreement with experiment. In contrast to previous theoretical treatments of $[VOCl_4]^{2-}$, which predict the reversed order of the first two absorptions, the DVXα results yield the correct energy-level scheme. The ESR *g* and *A* values for this species are also well reproduced theoretically.

Vanadium(IV) chemistry is dominated by the vanadyl ion, VO^{2+}, with relatively few examples of straight V^{4+} complexes. The strongly bound oxygen atom of vanadyl species exerts a profound influence on their spectral and magnetic properties.[1] The formally d^1 electron configuration implies a relatively simple electronic structure and a large number of experimental and theoretical studies[2–15] have attempted to rationalise the absorption and ESR spectra of this class of compounds. Ballhausen and Gray[7] presented the first detailed theoretical analysis of the bonding in VO^{2+} complexes with their molecular orbital (MO) treatment of $[VO(OH_2)_5]^{2+}$. Despite the relatively crude approach, their scheme has formed the cornerstone of many subsequent publications.[2,8–15] The calculations on $[VO(OH_2)_5]^{2+}$ indicated[7,8] a significant V–O π interaction and gave the relative energies of the d functions as $d_{xy} < d_{xz}$, $d_{yz} < d_{x^2-y^2} < d_{z^2}$ (or $b_2 < e < b_1 < a_1$ in C_{4v} symmetry). The three lowest-energy electronic transitions were assigned to d–d bands labelled I, II and III for the one-electron promotions from d_{xy} to $d_{x^2-y^2}$, (d_{xz}, d_{yz}) and d_{z^2} respectively.

Since this pioneering study there has been considerable disagreement over the energies and assignments of the d–d transitions in vanadyl systems. However, detailed low-temperature spectroscopic measurements on single crystals using polarised light appear to have resolved many of these issues.[2] Thus, for five co-ordinate VO complexes the charge transfer (c.t.) bands generally appear above the d–d transitions with the d–d band energies somewhat lower than 30 000 cm^{-1}. The singly occupied orbital is invariably b_2 (d_{xy}) which is essentially non-bonding. The highest-energy d orbital is the a_1 function (d_{z^2}) due to the very strong destabilising effect of the V–O σ bond. The general pattern is unaltered by the addition of a sixth ligand *trans* to the vanadyl oxygen. The transition to a_1, band III, moves to higher energy (> 30 000 cm^{-1}) and may be masked by c.t. absorptions. The relative positions of the b_1 ($d_{x^2-y^2}$) and e (d_{xz}, d_{yz}) levels, which are associated with bands I and II respectively, are mainly determined by a balance between the σ-donor strength of the equatorial ligand and the V–O π bonding. For $[VOCl_4]^{2-}$, for example, bands I and II are located at 11 600 and 13 700 cm^{-1} respectively,[2] which is the reverse of the Ballhausen–Gray scheme for $[VO(OH_2)_5]^{2+}$.

The complex $[CrOCl_4]^-$ seemed, until recently, to present quite a different picture from its isoelectronic analogue $[VOCl_4]^{2-}$.[16] Only two bands had been observed below 30 000 cm^{-1} for the chromium system with just the lower of the two assigned to a d–d transition. The higher-energy band was thought to be c.t. in origin although this conclusion was based largely on two theoretical studies[17,18] which agreed on the c.t. nature of this band but disagreed on its detailed assignment. However, new experimenetal evidence has been obtained by Collison[19] who located a third band below 30 000 cm^{-1} and assigned all three low-energy transitions to d–d absorptions. This assignment was confirmed theoretically in this laboratory using the discrete variational Xα (DVXα) model.[20]

The quantitative success of the DVXα calculation on $[CrOCl_4]^-$ extends to the spectra and bonding in chlorocuprate(II) species,[21] plus other studies on a variety of metal complexes,[22–25] organometallic compounds[26–28] and clusters.[29–31] The present work seeks to carry this success still further by examining the spectral properties and bonding for several vanadium(IV) complexes. The molecules studied include the simple binary halides VCl_4 and $[VCl_5]^-$, which provide some useful guides to the model's treatment of the V–Cl bond, together with the six vanadyl species $[VOCl_4]^{2-}$, $[VO(NCS)_4]^{2-}$, $[VO(NCS)_4(OH_2)]^{2-}$, $[VO(CN)_5]^{3-}$, $[VO\{OC(NH_2)_2\}_2Cl_2]$ and $[VO(NMe_3)_2Cl_2]$. The present work shows the DVXα scheme's quantitative accuracy for both small and large molecules. In particular, one need not resort to artificially truncated model systems. The uniform application of the DVXα approach to these systems provides a deeper insight into the complex electronic structures, bonding and spectral properties of d^1 V^{4+} and VO^{2+} compounds.

Computational Details

The Density Functional Theorem provides a rigorous basis for the *exact* calculation of the ground-state electron density of any molecule. Such a treatment would include *all* possible electron exchange/correlation interactions. Unfortunately, the theorem merely proves that such an exact functional exists not how to generate it. Practical computational procedures therefore employ approximations to this hypothetical exact functional. One such scheme is the DVXα model. It is a relatively fast, numerical, local-density approach enjoying considerable success with

* *Supplementary data available* (No. SUP 56817, 15 pp.): molecular orbital energies and atomic orbital compositions. See Instructions for Authors, *J. Chem. Soc., Dalton Trans.*, 1991, Issue 1, pp. xviii–xxii.
Non-SI units employed: au ≈ 4.36 × 10^{-18} J, eV ≈ 1.60 × 10^{-19} J.

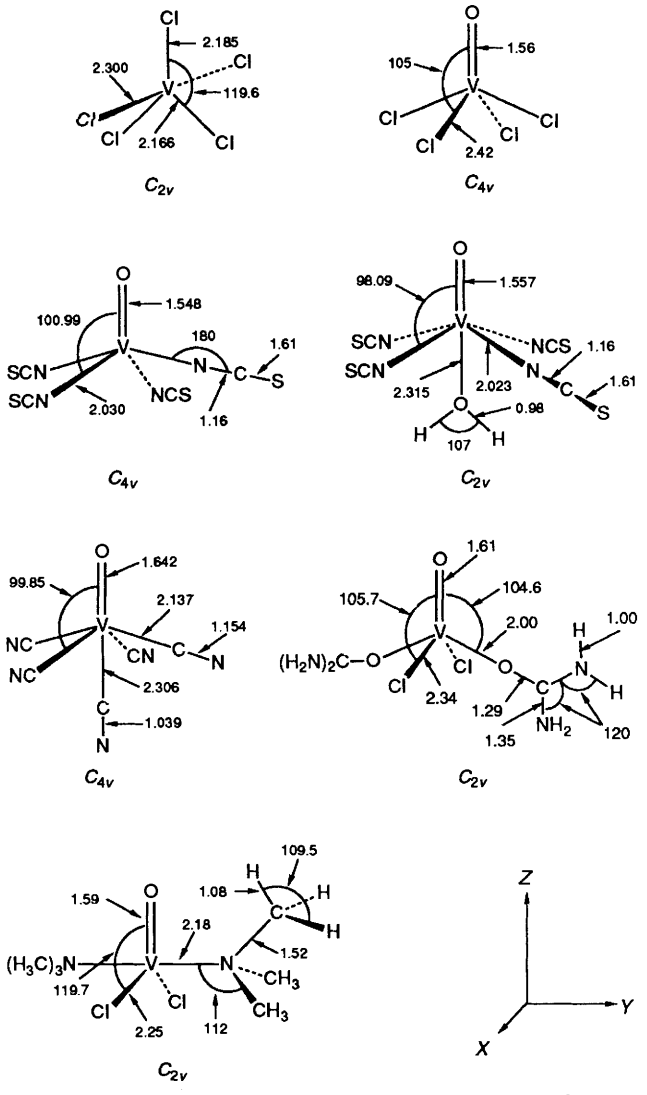

Fig. 1 Partially idealised molecular geometries (lengths in Å, angles in °) used in this work

transition-metal systems where more traditional methods based on Hartree–Fock theory struggle. The method gives accurate results for a range of metal systems and has been described in detail elsewhere.[32] Only those details relevant to the present study are included here.

Three levels of approximation have been applied. The first is the so-called self-consistent charge (SCC) scheme[33] within a spin-restricted formalism. The second is identical to the SCC method but within a spin-unrestricted scheme which allows for spin polarisation (SCCPOL). The final approach retains a spin-polarised framework but replaces the simple SCC approximation with a more accurate least-squares multipolar fit to the Coulomb potential (DVMPOL).[34] The latter calculations employ all multipoles up to $l = 1$ for all atoms except hydrogen where only $l = 0$ multipoles are used. There are seven radial functions for each multipole.

Near-minimal single site orbital (SSO) basis sets[35] were employed (up to 4p on V, up to 2p on O, N and C up to 3p on Cl and 1s on H) with the core functions (up to 3p V, 1s on O, C and N up to 2p on Cl) frozen[36] and orthogonalised against the valence orbitals. The SSO basis sets, which are of approximately double-ζ quality,[35] were further constrained by applying an external potential well of depth -2 au, with inner and outer radii of 4 and 6 au repectively for V and Cl and 2 and 4 au respectively for O, C, N and H. The basis sets were optimised as previously described[21] for both SCC and DVMPOL calculations. Basis-set populations from SCCPOL calculations were not significantly different from the simpler SCC results so no further optimisation was required.

Sampling points were distributed such that *ca.* 1100 points were associated with V, 500–600 points with C, N and O, 300 points with H and 600–700 points with Cl. This distribution scheme ensures a numerical error of approximately ±0.02 eV in molecular orbital energies and ±0.002 in atomic orbital populations, relative to the limit of a very large number of sampling points.

All charge densities and orbital populations are based on Mulliken analyses.[37] Estimates of the transition energies were computed using Slater's transition-state formalism.[38] In this procedure, a calculation is performed using MO occupations corresponding to the halfway point in the transition. Transition-state data are generally in better agreement with experiment than Xα MO energy differences, particularly if significant electronic relaxation accompanies the excitation.

Structural Details

The structures and geometries of all the compounds examined in this study, except the tetrahedral VCl_4 molecule, are shown schematically in Fig. 1. Bond lengths and angles have been derived from reported structural data save for $[VOCl_4]^{2-}$. No detailed structural parameters are available for this complex, although it has been shown to be isomorphous with the titanium analogue.[39] The latter species has a C_{4v} square-pyramidal geometry and this symmetry has invariably been assumed for $[VOCl_4]^{2-}$. The actual bond lengths and angles used here have been derived from the structures of $[VOCl_4(OH_2)]^{2-}$[40] and $[CrOCl_4]^-$.[41] The former has a V–O distance of 1.60 Å and V–Cl distances of 2.42 Å. The absence of an axial water molecule in $[VOCl_4]^{2-}$ might be expected, on the basis of Pauling's electroneutrality principle, to lead to a slight enhancement of the V–O bonding. Bond distances of 1.56 and 2.42 Å have been chosen for the V–O and V–Cl bonds respectively. The O–V–Cl angle was assigned a value of 105°, similar to the value of 104.5° found for $[CrOCl_4]^-$.[41]

Electron diffraction studies of VCl_4 have yielded bond lengths of 2.04[42] and 2.14 Å.[43] The latter value is used here. The structures of the other molecules are essentially the experimental geometries, slightly idealised to either C_{4v} or C_{2v} symmetry as appropriate (see Fig. 1). Equivalent parameters within the relevant point groups are the simple arithmetic means of the experimental values. Data have been extracted from the X-ray structures of $[PCl_4][VCl_5]$,[44] $[NMe_4]_4[VO(NCS)_4][VO(NCS)_4(OH_2)]$,[45] $K_3[VO(CN)_5]$,[46] $[VO(tmu)_2Cl_2]$[47] (tmu = tetramethylurea) and $[VO(NMe_3)_2Cl_2]$.[5] The methyl groups of tmu were replaced by hydrogens and all the internal angles of the ligand were fixed at 120°. The V–N vector in $[VO(NMe_3)_2Cl_2]$ defines a local C_3 axis as do the N–C vectors. The H–C–H angles were fixed at 109.5°.

Results and Discussion

There are several theoretical studies of vanadyl systems although the majority are based on extended Hückel/Wolfsberg–Helmholtz models. These approximate MO methods often give a reasonable qualitative treatment of transition-metal complexes but their quantative success is limited. An all-electron multiple scattering Xα study of a large number of metal halide oxide complexes has been reported.[14] Although the muffin-tin potential approximation characteristic of the MSXα approach can sometimes lead to erroneous results, the overlapping spheres method is capable of very good accuracy. In the present case, however, the authors were obliged to guess the structures of many of the systems they examined due to a lack of experimental structural data. Hence, while the qualitative trends appear quite reasonable, the details of the electronic structures of these systems are sometimes in error simply

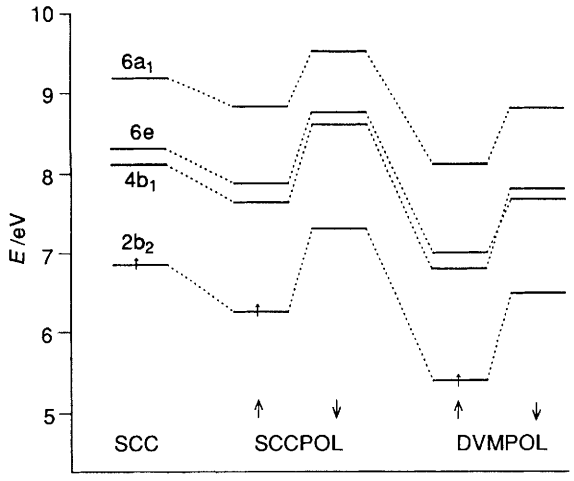

Fig. 2 Molecular orbital energy-level variations for $[VOCl_4]^{2-}$ as a function of the computational scheme

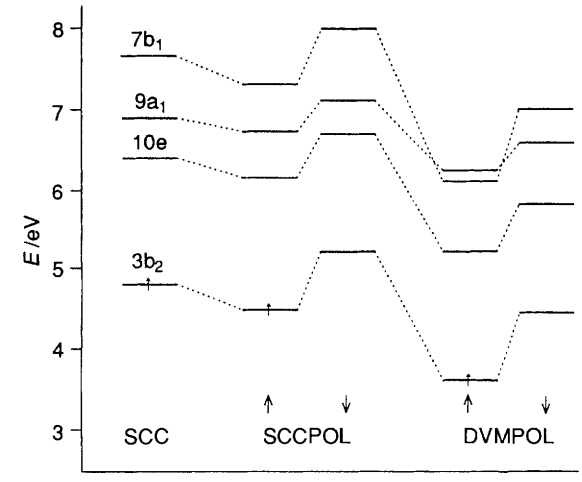

Fig. 3 Molecular orbital energy-level variations for $[VO(NCS)_4]^{2-}$ as a function of the computational scheme

because, as shown previously,[10,11] these quantities are sensitive to geometry. The present study therefore concentrates on complexes of known structure to avoid such problems as far as possible. The major exception is, of course, $[VOCl_4]^{2-}$ itself. This molecule has been the subject of so many studies that its inclusion here seems mandatory.

Choice of Computational Procedure.—Previous spin-unpolarised SCC calculations on chlorocuprates(II)[21] and $[CrOCl_4]^{-}$[20] yielded very satisfactory reproduction of the d–d and c.t. spectra. The same methodology was therefore applied to the present vanadium species. Again, near-quantitative reproduction of the d–d transition energies for the chloride-containing complexes results. However, as discussed below, band I for the thiocyanate and cyanide molecules is calculated rather too high in energy while band III is too low. Although this worsened the agreement with experiment for $[VO(NCS)_4(OH_2)]^{2-}$ and $[VO(CN)_5]^{3-}$, the computed and observed band assignments still concur. For $[VO(NCS)_4]^{2-}$, on the other hand, band III is predicted to fall below band I contrary to experiment. The simple SCC procedure appears to be inadequate in this instance and a more accurate scheme is required.

The SCCPOL and DVMPOL procedures represent progressive improvement of the computational method. The effect on the calculated energies for the mainly d-orbital MOs is shown schematically for $[VOCl_4]^{2-}$ in Fig. 2 and for $[VO(NCS)_4]^{2-}$ in Fig. 3. Fig. 2 indicates that the theoretical MO energies for the up-spin (α) functions of $[VOCl_4]^{2-}$ decrease fairly uniformly as a function of the method used. The relative ordering of, and energy differences between, the MOs remain pretty much intact. (Similar qualitative behaviour is shown by all the chloride-containing molecules.) The α-spin MOs of $[VO(NCS)_4]^{2-}$ also decrease as the level of approximation is improved but the energy of the $9a_1(\alpha)$ level changes much less rapidly than those of the other orbitals. In fact, for the DVMPOL approach, the $9a_1$ and $7b_1$ MOs swap over. This brings $[VO(NCS)_4]^{2-}$ back into qualitative agreement with experiment whereas, at the SCC level, experiment and theory diverge. Since a comparable level of approximation is required in order to make consistent predictions across the whole series of complexes, DVMPOL calculations were carried out for all the remaining molecules as well. Thus, unless specific comment is made to the contrary, all the following results are derived from DVMPOL computations.

Table 1 Complete listing of DVMPOL MO energies and their AO percentage compositions for VCl_4

			V			Cl	
MO	Spin	*E*/eV	3d	4s	4p	3s	3p
$5t_2$	↓	7.8762	3.8	—	86.5	1.5	8.2
$5t_2$	↑	7.5985	3.2	—	86.4	1.5	8.8
$3a_1$	↓	5.5113	—	88.6	—	1.4	9.9
$3a_1$	↑	5.2527	—	87.3	—	1.6	11.0
$4t_2$	↓	−2.8893	65.2	—	5.5	0.5	28.9
$4t_2$	↑	−3.5619	59.6	—	4.7	0.4	35.3
2e	↓	−3.8795	75.7	—	—	—	24.3
2e *	↑	−4.6124	68.6	—	—	—	31.4
$1t_1$	↓	−7.6547	—	—	—	—	100.0
$1t_1$	↑	−7.6550	—	—	—	—	100.0
$3t_2$	↓	−8.7477	0.6	—	6.9	0.6	91.8
$3t_2$	↑	−8.7899	0.7	—	7.5	0.7	91.2
1e	↓	−9.2922	24.3	—	—	—	75.7
$2t_2$	↓	−9.3511	27.4	—	−0.2	2.6	70.2
1e	↑	−9.5078	31.4	—	—	—	68.6
$2a_1$	↓	−9.6031	—	8.0	—	4.3	87.7
$2t_2$	↑	−9.6271	33.2	—	−0.1	3.1	63.8
$2a_1$	↑	−9.7049	—	8.8	—	4.7	86.5
$1t_2$	↓	−20.2562	3.0	—	1.3	94.8	0.9
$1t_2$	↑	−20.2903	3.4	—	1.5	94.2	0.9
$1a_1$	↓	−20.6943	—	3.4	—	94.2	2.4
$1a_1$	↑	−20.7289	—	3.9	—	93.7	2.4

* HOMO.

Ground State Electronic Structures.—Most of the following discussion centres on the MOs of predominantly d-orbital character. The DVMPOL calculations always predict the correct ground state: the unpaired electron resides in the mainly d_{xy} function for the C_{4v} VO^{2+} molecules or in $d_{x^2-y^2}$ for the C_{2v} vanadyl species. For VCl_4 and $[VCl_5]^{-}$ the electron is in the degenerate e $d_{x^2-y^2}$, d_{xy} functions and the d_{xz} orbital respectively. Since the spin is located mainly in the d levels, the largest spin polarisation splitting of α- and β-spin MOs is found for these functions also. The magnitude of the splitting is generally of the order of 0.6–0.8 eV and, for a given pair of spin orbitals, is roughly proportional to the average d atomic orbital component.

VCl_4. Vanadium tetrachloride has been the subject of various theoretical studies[48,49] including an early application of an *ad hoc* DVXα SCC method.[50] Although the details of the computed energy levels differ slightly, the qualitative description of the electronic structure is the same. The data in Table 1 show that the lowest two levels, $1a_1$ and $1t_2$, correspond to the Cl 3s orbitals followed by a set of levels ($2a_1$ to $1t_1$) which are mainly Cl 3p in nature. Above these are the vanadium d orbitals 2e and $4t_2$ then the $3a_1$ 4s orbital and finally the $5t_2$ 4p levels. The chloride ligands bind mainly *via* their 3p orbitals with the 1e and $2t_2$ bonding functions showing about 30% V d to 70% Cl 3p character. This reasonably large covalent mixing is mirrored

Table 2 Partial listing of DVMPOL MO energies and their AO percentage compositions for $[VCl_5]^-$. Complete listing in SUP 56817

			V			Cl_{eq}		Cl_{ax}	
MO	Spin	*E*/eV	3d	4s	4p	3s	3p	3s	3p
$10a_1$	↓	2.9729	65.4	0.1	0.0	0.5	10.9	0.8	22.4
$10a_1$	↑	2.2084	57.4	0.1	0.0	0.5	13.5	0.7	27.9
$9a_1$	↓	1.5724	70.4	0.1	4.1	0.4	23.7	0.0	1.3
$6b_2$	↓	1.4057	72.9	—	2.7	0.3	23.1	—	1.0
$3a_2$	↓	0.8108	81.2	—	—	—	7.8	—	11.0
$6b_1$	↓	0.8022	81.2	—	0.0	—	6.7	0.0	12.1
$9a_1$	↑	0.7831	62.2	0.1	3.5	0.3	31.8	0.0	2.1
$6b_2$	↑	0.6013	64.3	—	2.2	0.3	31.6	—	1.7
$3a_2$	↑	−0.0608	71.6	—	—	—	9.8	—	18.6
$6b_1$ *	↑	−0.0692	71.0	—	0.0	—	8.1	0.0	20.9
$2a_2$	↑	−1.4517	2.5	—	—	—	39.0	—	58.5
$2a_2$	↓	−1.4653	1.4	—	—	—	33.7	—	65.0

* HOMO.

in the antibonding 'ligand field' 2e and $4t_2$ levels which display the reversed compositions of about 70% V d to 30% Cl 3p. The $4t_2$ levels show a slightly greater degree of mixing consistent with their larger σ-bonding role and concomitant higher energy. The ground state is computed to be ^2E as expected from elementary ligand-field theory arguments.

$[VCl_5]^-$. No previous *ab initio* calculations of this complex appear to have been published although $[VCl_5]^-$ has been the subject of both crystal field theory (c.f.t.) and angular overlap model (a.o.m.) treatments.[51] Both models were used in an attempt to predict the symmetry of the $[VCl_5]^-$ anion on the basis of the d–d band energies. The c.f.t. analysis was consistent with a square-pyramidal geometry while the a.o.m. gave the (correct) trigonal-bipyramidal stereochemistry. The cellular ligand field (c.l.f.) model has also been applied to $[VCl_5]^-$.[52] The c.l.f. analysis was under-determined but still leads to the prediction that the equatorial chlorides donate more strongly than do the axial chlorides, consistent with the shorter bond lengths for the former.

A full listing of the DVMPOL MO energies and atomic orbital (AO) compositions is given in SUP56817. Table 2 lists only those data relevant to the MOs with mainly d-orbital character and the next level to lower energy. These comprise the occupied $2a_2(\alpha)$ and $2a_2(\beta)$ levels, the $6b_1(\alpha)$ highest occupied MO (HOMO) and the nine virtual functions $6b_1(\beta)$, $3a_2(\alpha)$, $3a_2(\beta)$, $6b_2(\alpha)$, $6b_2(\beta)$, $9a_1(\alpha)$, $9a_1(\beta)$, $10a_1(\alpha)$ and $10a_1(\beta)$ immediately above. The composition of these functions reflects their M–L bonding roles. For the α-spin MOs, for example, the $2a_2$ level is essentially non-bonding while the $6b_1$ and $3a_2$ MOs are of V–Cl π symmetry with ≈30% admixture of chlorine character. The axial chlorides account for about two thirds of the total ligand-based component. The $6b_2$ and $9a_1$ orbitals are of σ symmetry with respect to the equatorial donors leading to an increased Cl_{eq} contribution of 32% with only a 2% participation of the axial chlorines. The $10a_1$ MO describes both equatorial and axial σ bonding with a 41% ligand component. The axial ligands contribute about twice as much to the $10a_1$ level as the equatorial Cl reflecting the spatial distribution of the d_{z^2} function. The d-orbital components mirror the M–L bonding roles also. Thus, for the π-bonding $6b_1$ and $3a_2$ orbitals, the equatorial σ-bonding $6b_2$ and $9a_1$ levels and the equatorial and axial σ-bonding $10a_1$ function the d component decreases from ≈71 to 63 to 57% respectively. This increasing covalence also leads to an increase in the energies of these antibonding MOs.

$[VOCl_4]^{2-}$. Several extended-Hückel calculations of the electronic structure and bonding in $[VOCl_4]^{2-}$ have appeared. Molecular orbital energies have been computed in both C_{4v}[10] and C_{2v}[11] symmetries yielding results in qualitative agreement with the original Ballhausen–Gray model but in relatively poor agreement with experiment. A more accurate overlapping-spheres MSXα treatment has been reported.[14] This method is roughly equivalent to the DVXα SCC procedure and both approaches gives results of similar accuracy.[21]

The latest spectroscopic measurements on $[CrOCl_4]^-$[19] closely correlate with the data for the vanadyl analogue. It is therefore not surprising that the calculated electronic structures for these two complexes are virtually identical. The energies and AO compositions of the MOs are collected in Table 3. The $2b_2(\alpha)$ HOMO leads to the correct $^2B_2$ ground state. This function is essentially a non-bonding d_{xy} orbital although a 14.4% Cl contribution arises from a weak π interaction in the equatorial plane. This interaction depends on the O–V–Cl angle and decreases as this angle widens. The $4b_1$ functions, corresponding to the $d_{x^2-y^2}$ orbital, have about 31% Cl 3p character with ligand components of both σ and π symmetries. The 6e orbitals monitor the V–O π bond with the d component reduced by 1% relative to the $4b_1$ levels. The highest-energy d-type MO for each spin ($6a_1$) describes the main V–O σ antibonding orbital. It has, as expected, the smallest d component (only 54.7%) with significant admixtures of vanadium 4s and oxygen $2p_z$ functions. There is a lesser contribution from the equatorial Cl ligands commensurate with the longer and weaker V–Cl bonding and with the relative size of the d_{z^2} 'belly band'. Aside from an inversion of the $4b_1$ and 6e levels, the descriptions of the mainly d MOs for $[VOCl_4]^{2-}$ and $[CrOCl_4]^-$ are very similar. The qualitative order of the lower-lying occupied MOs is also closely parallel. In particular, the 10 functions immediately below the HOMO are Cl non-bonding levels. Below these are the eight V–Cl bonding levels of which the $2b_1$ and $1b_2$ are the most important. Then come the V–O σ and π bonding orbitals $3a_1$ and 2e respectively. At much lower energies are the essentially unperturbed Cl 3s orbitals and finally the $1a_1$ functions describing the oxygen 1s orbital. The orbital mixings show that Cl mainly employs its 3p functions for bonding (*cf.* VCl_4 and $[VCl_5]^-$). The larger mixing in the $2b_1$ levels, which are mainly of V–Cl(σ) symmetry, compared to the $1b_2$ levels, which are of V–Cl(π) symmetry, suggests that V–Cl σ bonding is larger than V–Cl π bonding. The vanadyl V–O bond, on the other hand, has roughly equal orbital mixings in its σ- and π-symmetry bonding MOs. Relative to the V–Cl bond, therefore, the V–O interaction has a greatly enhanced π-bonding component.

$[VO(NCS)_4]^{2-}$. The orbital mixing in $[VO(NCS)_4]^{2-}$, as measured by the d-orbital compositions in Table 4, is generally greater than for either $[VCl_5]^-$ or $[VOCl_4]^{2-}$. (A complete listing of all the MO energies and compositions has been deposited in SUP 56817.) The overall greater covalency for the thiocyanate complex squares well with the stronger donor properties expected for NCS^- relative to Cl^-. However, the electronic structure of $[VO(NCS)_4]^{2-}$ while broadly similar to

Table 3 Complete listing of DVMPOL MO energies and their AO percentage compositions for $[VOCl_4]^{2-}$

			V			O		Cl	
MO	Spin	*E*/eV	3d	4s	4p	2s	2p	3s	3p
$8a_1$	↓	19.1758	12.2	17.6	63.3	2.4	3.6	0.0	0.8
$8a_1$	↑	18.8657	10.5	18.0	63.6	2.9	4.1	0.0	1.0
7e	↓	17.6521	0.0	—	92.9	—	2.4	0.6	4.0
7e	↑	17.3109	0.0	—	91.6	—	2.9	0.7	4.8
$7a_1$	↓	13.6987	−0.1	68.2	20.5	0.1	0.6	0.9	9.8
$7a_1$	↑	13.2684	−0.1	66.0	20.9	0.1	0.7	1.1	11.3
$6a_1$	↓	8.8367	60.2	2.6	12.4	0.2	16.8	0.2	7.6
$6a_1$	↑	8.0817	54.7	2.3	10.8	0.2	22.4	0.2	9.3
$4b_1$	↓	7.8175	77.1	—	—	—	—	0.8	22.1
6e	↓	7.7863	76.8	—	0.0	—	17.8	0.1	5.2
6e	↑	6.9503	67.2	—	0.1	—	25.6	0.1	6.9
$4b_1$	↑	6.8535	68.3	—	—	—	—	0.8	31.0
$2b_2$	↓	6.4822	91.5	—	—	—	—	—	8.5
$2b_2$*	↑	5.3654	85.6	—	—	—	—	—	14.4
$1a_2$	↑	3.8042	—	—	—	—	—	—	100.0
$1a_2$	↓	3.7877	—	—	—	—	—	—	100.0
5e	↑	3.3331	0.2	—	0.1	—	1.8	0.0	97.9
5e	↓	3.3214	0.3	—	0.0	—	1.0	0.0	98.7
$3b_1$	↑	3.2147	0.2	—	—	—	—	0.0	99.8
$3b_1$	↓	3.2046	0.2	—	—	—	—	0.0	99.7
4e	↑	3.0085	0.4	—	0.0	—	6.4	0.0	93.2
4e	↓	2.9759	0.1	—	0.0	—	6.1	0.0	93.8
$5a_1$	↑	2.5120	0.2	0.1	2.6	0.2	4.4	0.0	92.4
$5a_1$	↓	2.5059	0.4	0.1	2.5	0.1	2.8	0.0	94.1
$2b_1$	↓	2.0766	21.4	—	—	—	—	0.4	78.1
3e	↓	2.0005	2.5	—	4.1	—	0.6	0.5	92.3
$1b_2$	↓	1.9838	8.5	—	—	—	—	—	91.5
3e	↑	1.9395	1.9	—	5.5	—	2.3	0.6	89.7
$1b_2$	↑	1.8757	14.4	—	—	—	—	—	85.6
$2b_1$	↑	1.7894	30.0	—	—	—	—	0.7	69.3
$4a_1$	↓	1.3197	1.6	9.3	0.5	0.1	1.6	1.4	85.4
$4a_1$	↑	1.2296	0.1	10.4	0.9	0.5	7.8	1.4	78.7
2e	↓	0.8148	20.2	—	2.0	—	72.0	0.0	5.8
2e	↑	0.7984	30.1	—	1.7	—	61.0	0.0	7.2
$3a_1$	↓	0.7282	21.1	−0.1	0.5	2.9	73.8	0.1	1.6
$3a_1$	↑	0.6889	29.2	0.3	0.6	3.5	59.5	0.3	6.6
$1b_1$	↑	−8.5499	1.5	—	—	—	—	98.5	0.0
$1b_1$	↓	−8.5517	1.2	—	—	—	—	98.8	0.0
1e	↑	−8.7108	0.2	—	1.0	—	0.0	98.5	0.2
1e	↓	−8.7150	0.2	—	0.9	—	0.0	98.8	0.2
$2a_1$	↓	−9.0130	0.4	1.6	0.1	0.1	0.0	97.3	0.5
$2a_1$	↑	−9.0178	0.5	1.8	0.2	0.1	0.0	96.9	0.5
$1a_1$	↑	−12.6058	4.8	1.0	0.4	92.5	1.0	0.1	0.1
$1a_1$	↓	−12.9022	4.1	0.8	0.2	94.0	0.8	0.1	0.1

* HOMO.

Table 4 Partial listing of DVMPOL MO energies and their AO percentage compositions for $[VO(NCS)_4]^{2-}$. Complete listing in SUP 56817

			V			O		N		C		S	
MO	Spin	*E*/eV	3d	4s	4p	2s	2p	2s	2p	2s	2p	3s	3p
$7b_1$	↓	6.9684	74.1	—	—	—	—	11.8	6.3	2.9	2.4	0.0	2.4
$9a_1$	↓	6.5990	29.1	0.0	17.8	0.0	10.6	0.5	6.2	0.2	26.9	0.0	8.7
$9a_1$	↑	6.2303	33.2	0.0	17.4	0.1	16.0	0.8	3.7	0.2	20.9	0.0	7.7
$7b_1$	↑	6.1723	72.6	—	—	—	—	13.5	7.9	2.5	1.6	0.0	1.9
10e	↓	5.7784	65.9	—	0.0	—	19.8	1.2	1.4	0.2	8.1	0.0	3.6
10e	↑	5.2048	61.7	—	0.1	—	27.1	1.4	1.1	0.2	5.4	0.0	3.1
$3b_2$	↓	4.3677	74.9	—	—	—	—	—	0.3	—	12.9	—	11.9
$3b_2$*	↑	3.6272	71.5	—	—	—	—	—	2.3	—	10.0	—	16.2
$2a_2$	↓	1.9962	—	—	—	—	—	—	27.3	—	1.2	—	71.5
$2a_2$	↑	1.9872	—	—	—	—	—	—	27.3	—	1.4	—	71.3

* HOMO.

$[VOCl_4]^{2-}$ is more complex. Within the notional d-orbital set, the d_{z^2} function is now no longer localised mainly in one pair of α- and β-spin MOs but provides a fairly large contribution to both the $9a_1$ and $10a_1$ levels. The d-orbital contribution to $9a_1$ is less than half that of any other mainly d level. This difference correlates with the behaviour of the MO energies as a function of the computational procedure. Recall from Fig. 3 that the $9a_1(\alpha)$ level drops much less rapidly than the remaining d-type MOs. It appears, then, that if an SCC calculation results in very different d-orbital contributions to the mainly d MOs, then a

Table 5 Partial listing of DVMPOL MO energies and their AO percentage compositions for $[VO(NCS)_4(OH_2)]^{2-}$. Complete listing in SUP 56817

			V			O		N		C		S		$O(H_2)$		H
MO	Spin	*E*/eV	3d	4s	4p	2s	2p	2s	2p	2s	2p	3s	3p	2s	2p	1s
$9a_2$	↓	7.7242	73.5	—	—	—	—	11.5	6.1	3.4	2.6	0.0	2.8	—	—	—
$14a_1$	↓	7.6113	17.6	0.1	11.4	0.0	5.4	0.6	14.2	0.2	34.8	0.0	8.7	1.5	0.0	5.3
$14a_1$	↑	7.3541	24.2	0.1	11.8	0.0	10.0	1.1	10.6	0.4	28.0	0.0	7.6	1.5	0.0	4.7
$9a_2$	↑	6.9200	73.2	—	—	—	—	13.2	7.3	2.9	1.3	0.0	2.0	—	—	—
$11b_2$	↓	6.4167	64.5	—	0.1	—	20.6	0.8	1.8	0.1	8.6	0.0	3.2	—	0.2	—
$11b_1$	↓	6.3925	63.6	—	0.2	—	20.6	0.9	1.9	0.1	8.9	0.0	3.3	—	0.1	0.4
$11b_2$	↑	5.8655	60.4	—	0.3	—	28.9	1.1	1.1	0.1	5.4	0.0	2.5	—	0.2	—
$11b_1$	↑	5.8527	59.6	—	0.3	—	29.0	1.1	1.2	0.2	5.7	0.0	2.6	—	0.0	0.3
$13a_1$	↓	4.9555	74.1	0.0	0.0	0.0	0.0	0.0	0.0	0.0	14.9	0.0	11.0	0.0	0.0	0.0
$13a_1$ *	↑	4.2048	73.1	0.0	0.0	0.0	0.0	0.0	1.1	0.0	11.5	0.0	14.2	0.0	0.0	0.0
$8a_2$	↓	2.2637	0.0	—	—	—	—	0.0	26.9	0.0	1.2	0.0	71.9	—	—	—
$8a_2$	↑	2.2565	0.0	—	—	—	—	0.0	26.8	0.0	1.4	0.0	71.8	—	—	—

* HOMO.

Table 6 Partial listing of DVMPOL MO energies and their AO percentage compositions for $[VO(CN)_5]^{3-}$. Complete listing in SUP 56817

			V			O		C(eq.)		N(eq.)		C(ax.)		N(ax.)	
MO	Spin	*E*/eV	3d	4s	4p	2s	2p	2s	2p	2s	2p	2s	2p	2s	2p
$10a_1$	↓	14.5859	14.3	0.9	8.0	−0.1	1.9	2.6	34.5	0.0	26.4	7.4	4.1	−0.1	0.1
$5b_1$	↓	14.4906	63.2	—	—	—	—	20.2	11.7	−0.1	5.0	—	—	—	—
$10a_1$	↑	14.3381	25.5	0.9	7.2	0.0	5.5	4.9	23.4	0.0	17.6	9.6	5.3	−0.1	0.2
$5b_1$	↑	13.7460	59.9	—	—	—	—	24.4	12.1	−0.2	3.7	—	—	—	—
8e	↓	12.4898	62.4	—	0.0	—	19.1	2.2	6.0	0.0	8.0	—	0.8	—	1.6
8e	↑	11.9386	57.4	—	−0.1	—	28.6	2.9	4.2	0.0	5.5	—	0.4	—	1.0
$2b_2$	↓	10.9598	80.3	—	—	—	—	—	3.2	—	16.5	—	—	—	—
$2b_2$ *	↑	10.0875	83.9	—	—	—	—	—	1.1	—	15.1	—	—	—	—
$9a_1$	↑	8.2242	1.1	0.1	5.1	0.2	25.2	2.1	2.9	0.1	8.5	21.0	24.1	1.2	8.5
$9a_1$	↓	8.1905	2.0	0.0	4.8	0.1	18.6	2.3	3.5	0.2	9.3	22.4	26.1	1.4	9.4

* HOMO.

DVMPOL procedure is required. Conversely, if the SCC calculation yields essentially similar d-orbital contributions, no significant gain will obtain from the more accurate approach.

The data in Table 4 again provide some insights into the nature of the metal–ligand bonding. The $3b_2(\alpha)$ MO shows a 28.5% contribution from the NCS p_π orbitals indicating a similar degree of π bonding to that from Cl in $[VOCl_4]^{2-}$. The $10e(\alpha)$ of $[VO(NCS)_4]^{2-}$ also matches the 6e level of $[VOCl_4]^{2-}$ with ligand components dominated by the vanadyl oxygen p_π orbitals (27.1%). The $7b_1(\alpha)$ MO reflects the in-plane V–NCS bonding with most of the ligand contribution of 21.4% arising from nitrogen orbitals. The $9a_1(\alpha)$ function has significant contributions from V d_{z^2} (33.2%), V 4p (17.4%), O 2p (16.0%) and C 2p (20.9%). The presence of a large admixture of NCS character into the a_1 MOs evidently leads to the overall greater covalence in the V–NCS compared to the V–Cl bond and is the major difference between the two interactions.

$[VO(NCS)_4(OH_2)]^{2-}$. The addition of a water ligand to $[VO(NCS)_4]^{2-}$ has a relatively small effect on the overall electronic structure (Table 5 and SUP 56817). The water ligand orbitals do not mix significantly with any metal functions, the largest interaction being located in the $6a_1(\alpha, \beta)$ MOs in which there is ≈11% metal and ≈22% OH_2 character. No doubt, this result is due to the rather long V–OH_2 bond length of 2.32 Å. The compositions of the antibonding MOs describing the V–O and V–NCS bonding in $[VO(NCS)_4(OH_2)]^{2-}$ (Table 5) and $[VO(NCS)_4]^{2-}$ (Table 4) are generally quite similar, noting that the e orbitals in C_{4v} symmetry transform as b_1 and b_2 orbitals in C_{2v}. The $14a_1$ function of the aqua species has an even smaller d_{z^2} component (24.2%) than that in the corresponding $9a_1$ function of $[VO(NCS)_4]^{2-}$ (33.2%). In addition, the $14a_1$ orbital has been destabilised by 0.5 eV relative to the comparable energy difference in the unhydrated species. This leads to a large increase in the band III energy for the hydrate.

$[VO(CN)_5]^{3-}$. Table 6 gives the energies and compositions of the mainly d MOs for $[VO(CN)_5]^{3-}$. A full listing is available in SUP 56817. Conventional chemical arguments have cyanide binding more strongly than either Cl^- or NCS^-, a view generally supported by the present DVXα calculations. The d-orbital contributions to $5b_1$, 8e and $10a_1$ are all smaller than their counterparts in $[VOCl_4]^{2-}$ or $[VO(NCS)_4]^{2-}$. In fact, the $10a_1(\alpha)$ function now has only 25.5% d_{z^2} character. The $11a_1(\alpha)$ orbital some 1.3 eV higher in energy has a greater share of d_{z^2} (32.4%). Both levels have a much greater contribution from the equatorial CN^- ligands than from the axial CN^- group. The V–CN bond is unusual in that it results in a $2b_2(\alpha)$ d_{xy} component which is larger than that for the $2b_2(\beta)$ function. The opposite is found for all the other molecules. This result appears to stem from the π-acceptor nature of the V–CN bonding *versus* the essentially π-donor roles for all the other ligands considered here, apart from NMe_3 which has no π interaction.

$[VO\{OC(NH_2)_2\}_2Cl_2]$. The $VOCl_2O_2$ core of $[VO\{OC(NH_2)_2\}_2Cl_2]$ approximates to C_{4v} symmetry although the MO energies and compositions in Table 7 (complete list in SUP 56817) indicate a greater contribution from Cl^- than urea. For example, the $15a_1(\alpha)$ function, which describes the main in-plane σ-antibonding interaction, has Cl and urea contributions of 18.2 and 9.2% respectively. The average d-orbital components indicate a slightly greater covalency for $[VO\{OC(NH_2)_2\}_2Cl_2]$ compared to $[VOCl_4]^{2-}$. A more important difference between $[VO\{OC(NH_2)_2\}Cl_2]$ and the other vanadyl complexes is that the mainly d-type MOs in the former are no longer clustered together in a single group. Urea-based functions of b_1 and a_2 symmetry fall below the $16a_1$ d_{z^2}-type levels. The spin-polarisation splitting of the mainly d-orbital MOs is sufficiently large for the β-spin partner of the $8b_1(\alpha)$ d_{xz} orbital to lie above both the α- and β-spin urea-based b_1 functions.

Table 7 Partial listing of DVMPOL MO energies and their AO percentage compositions for $[VO\{OC(NH_2)_2\}_2Cl_2]$. Complete listing in SUP 56817

			V			O		Cl		O(urea)		C		N		H
MO	Spin	*E*/eV	3d	4s	4p	2s	2p	3s	3p	2s	2p	2s	2p	2s	2p	1s
$16a_1$	↓	1.3284	61.1	0.9	11.1	0.3	17.9	0.1	4.5	0.7	1.5	0.4	0.8	0.2	0.3	0.4
$16a_1$	↑	0.6797	55.0	1.0	10.0	0.2	24.1	0.1	5.7	0.7	1.7	0.3	0.6	0.2	0.2	0.3
$15a_1$	↓	0.5626	77.3	−0.1	0.0	0.0	0.0	0.4	13.9	3.5	0.6	1.3	2.1	0.1	0.1	0.7
$6a_2$	↓	0.4432	19.4	—	—	—	—	—	0.1	—	21.7	—	42.8	—	16.1	—
$9b_1$	↓	0.3074	66.8	—	0.0	—	18.0	0.1	6.0	—	2.2	—	5.0	—	1.9	—
$12b_2$	↓	0.2675	76.1	—	0.0	—	18.8	—	0.2	0.9	2.2	0.3	0.7	0.2	0.2	0.3
$6a_2$	↑	0.2572	7.9	—	—	—	—	—	0.0	—	23.0	—	49.6	—	19.5	—
$8b_1$	↓	−0.0019	5.9	—	0.4	—	1.2	0.1	2.9	—	17.2	—	50.8	—	21.4	—
$9b_1$	↑	−0.0020	3.0	—	0.5	—	1.8	0.0	0.2	—	19.2	—	53.0	—	22.2	—
$15a_1$	↑	−0.3284	72.6	0.0	0.0	0.0	0.0	0.4	17.8	4.0	1.1	1.2	2.1	0.1	0.1	0.6
$8b_1$	↑	−0.4105	59.2	—	−0.1	—	26.2	0.1	10.6	—	0.6	—	2.3	—	1.1	—
$12b_2$	↑	−0.4435	66.7	—	0.2	—	27.8	—	0.3	1.0	2.5	0.3	0.6	0.1	0.2	0.2
$5a_2$	↓	−1.1879	69.1	—	—	—	—	—	10.2	—	0.5	—	12.6	—	7.6	—
$5a_2$*	↑	−2.0123	73.4	—	—	—	—	—	17.5	—	0.0	—	5.1	—	4.1	—
$7b_1$	↑	−3.9448	0.4	—	0.0	—	14.0	0.0	85.4	—	0.1	—	0.0	—	0.0	—
$7b_1$	↓	−3.9804	0.0	—	−0.1	—	11.5	0.0	88.4	—	0.0	—	0.0	—	0.0	—

* HOMO.

Table 8 Partial listing of DVMPOL MO energies and their AO percentage compositions for $[VO(NMe_3)_2Cl_2]$. Complete listing in SUP 56817

			V			O		Cl		N		C		H
MO	Spin	*E*/eV	3d	4s	4p	2s	2p	3s	3p	2s	2p	2s	2p	1s
$15a_1$	↓	0.9323	63.7	2.3	5.4	0.3	12.4	0.0	2.0	3.1	7.3	0.1	1.1	2.1
$15a_1$	↑	0.1886	57.8	2.1	5.2	0.3	17.2	0.0	2.4	3.2	8.7	0.1	0.9	2.1
$10b_1$	↓	−0.1514	71.0	—	0.5	—	17.5	0.4	10.6	—	0.0	0.0	0.0	0.0
$14a_1$	↓	−0.5436	71.9	0.3	4.3	0.0	4.1	0.3	14.0	0.9	3.2	0.1	0.3	0.7
$10b_1$	↑	−0.8906	62.7	—	0.2	—	23.8	0.4	12.9	—	0.0	0.0	0.0	0.0
$11b_2$	↓	−0.9692	76.6	—	0.8	—	19.0	—	2.3	0.1	0.2	0.2	0.7	0.2
$14a_1$	↑	−1.4020	65.5	0.2	3.4	0.0	4.6	0.3	18.1	1.3	5.2	0.1	0.3	1.0
$11b_2$	↑	−1.7405	66.8	—	0.9	—	28.0	—	2.9	0.2	0.4	0.1	0.5	0.2
$7a_2$	↓	−1.9969	89.2	—	—	—	—	—	9.4	—	0.0	0.3	1.0	0.2
$7a_2$*	↑	−3.0118	82.4	—	—	—	—	—	16.3	—	0.0	0.2	0.8	0.2
$9b_1$	↑	−5.3982	0.0	—	0.0	—	9.7	0.0	89.7	—	0.0	0.0	0.3	0.2
$9b_1$	↓	−5.4112	0.0	—	0.0	—	6.5	0.0	92.7	—	0.0	0.0	0.5	0.3

* HOMO.

Hence, the ligand orbitals comprise $9b_1(\alpha)$ and the $8b_1(\beta)$ while the mainly d orbitals are the $8b_1(\alpha)$ and the $9b_1(\beta)$ functions. The $7b_1$ levels immediately below the d set are composed mainly of Cl 3p orbitals.

The DVXα electronic structure can be compared with an extended-Hückel MO (EHMO) treatment.[12] The covalency, as measured by the squares of the EHMO d-orbital coefficients, is comparable to but somewhat less than that from the DVMPOL calculation. The MO energy differences are also comparable but the orders differ. The DVMPOL method predicts a d-orbital order of $d_{xy} < d_{yz} < d_{xz} < d_{x^2-y^2} < d_{z^2}$. The EHMO model reverses the order of d_{yz} and d_{xz}. The implication of this result is that the EHMO model leads to a stronger interaction from urea than from chloride. This also results in the EHMO model predicting that the MO immediately below the mainly d-orbital set is a urea-based function. The effects on the calculated absorption spectrum of the different strengths of the V–L interactions as well as the presence of the ligand-based levels amongst the metal d set of the DVMPOL calculation are discussed further below.

$[VO(NMe_3)_2Cl_2]$. The $[VO(NMe_3)_2Cl_2]$ MOs of mainly d-orbital character are again clustered together in a single group (Table 8, complete listing in SUP 56817). The overall covalency is comparable to that calculated for $[VOCl_4]^{2-}$ although, as for $[VO\{OC(NH_2)_2\}_2Cl_2]$, there are generally larger contributions from the Cl ligands. Moreover, the $9b_1$ orbitals immediately below the d levels are once again mainly Cl 3p in character. The geometry of $[VO(NMe_3)_2Cl_2]$ is approximately trigonal bi-pyramidal with obvious effects on the MO energy level order. Most notably, the $11b_2$ and $10b_1$ functions, which would be degenerate in C_{4v} symmetry, are split by 0.85 eV.

Total Charge and Spin Populations.—The nature of the metal–ligand bonding in these complexes can be probed in more detail *via* a Mulliken analysis of the ground-state charge density.[32] The total charge and spin populations for the metal and ligands are collected in Table 9. The most obvious feature of the total charges is that they are well removed from the notional values for the isolated components. For example, the vanadium ion has a formal charge of +4 which is reduced by about 3.5 units for VCl_4 and $[VCl_5]^-$ and by about 3 units for the VO^{2+} species, except for $[VO(CN)_5]^{3-}$ where the V charge is essentially zero. Most of this extra charge appears in the d orbitals. The formal V^{4+} $3d^14s^04p^0$ configuration changes to something like $3d^{3.30}4s^{0.25}4p^{0.45}$. The extra half an electron on the metal in VCl_4 and $[VCl_5]^-$ appears mainly in the 3d population while for $[VO(CN)_5]^{3-}$ the 4s and 4p orbitals accommodate the extra charge.

The increased charge accummulation on the metal must be at the expense of the ligands. For the vanadyl species the oxygen charge reduces from its formal value of −2 to around −0.4 to −0.5. This accounts for around half of the charge donation to the metal with the remaining 1.5 electrons coming from the equatorial (and axial) ligands. The large donation from the vanadyl oxygen is consistent with the strong, multiple V–O bonding. For the other ligands, an idea of the relative donor

Table 9 Total charges for the vanadium ion, the vanadyl oxygen and the ligands calculated *via* the DVMPOL procedure. The identity of the ligand is given in parentheses and all the corresponding spin populations are in italics

Complex	V	O	L^1	L^2
VCl_4	0.404	—	−0.101 (Cl)	—
	1.052	—	*−0.013*	—
$[VCl_5]^-$	0.499	—	−0.279 (Cl_{eq})	−0.331 (Cl_{ax})
	1.217	—	*−0.058*	*−0.022*
$[VOCl_4]^{2-}$	0.977	−0.483	−0.624 (Cl)	—
	1.320	*−0.232*	*−0.022*	—
$[VO(NCS)_4]^{2-}$	0.928	−0.372	−0.639 (NCS)	—
	1.074	*−0.202*	*0.032*	—
$[VO(NCS)_4(OH_2)]^{2-}$	1.042	−0.335	−0.668 (NCS)	0.046 (OH_2)
	1.083	*−0.220*	*0.035*	*−0.002*
$[VO(CN)_5]^{3-}$	−0.032	−0.533	−0.475 (CN_{eq})	−0.534 (CN_{ax})
	1.247	*−0.230*	*0.001*	*−0.026*
$[VO(NMe_3)_2Cl_2]$	0.707	−0.493	−0.425 (Cl)	0.318 (NMe_3)
	1.271	*−0.226*	*0.000*	*0.023*
$[VO\{OC(NH_2)_2\}_2Cl_2]$	0.956	−0.388	−0.475 (Cl)	0.191 (urea)
	1.175	*−0.257*	*0.008*	*0.033*

Table 10 Metal–ligand overlap populations from the DVMPOL calculations

Complex	V=O	V=O (σ)	V=O (π)	$V-L^1$	$V-L^2$
VCl_4	—	—	—	0.664	—
$[VCl_5]^-$	—	—	—	0.553 (Cl_{eq})	0.504 (Cl_{ax})
$[VOCl_4]^{2-}$	0.913	0.299	0.614	0.346 (Cl)	—
$[VO(NCS)_4]^{2-}$	0.953	0.325	0.628	0.465 (NCS)	—
$[VO(NCS)_4(OH_2)]^{2-}$	0.949	0.327	0.622	0.430 (NCS)	0.038 (OH_2)
$[VO(CN)_5]^{3-}$	0.901	0.289	0.612	0.628 (CN_{eq})	0.469 (CN_{ax})
$[VO(NMe_3)_2Cl_2]$	0.898	0.289	0.609	0.500 (Cl)	0.373 (NMe_3)
$[VO\{OC(NH_2)_2\}_2Cl_2]$	0.907	0.315	0.592	0.432 (Cl)	0.324 (urea)

strengths can be obtained from the total charge, providing one concentrates on a single ligand type. For example, the chloride charges increase in the series $VCl_4 < [VCl_5]^-(Cl_{eq}) < [VCl_5]^-(Cl_{ax})$ for the binary halides and $[VO(NMe_3)_2Cl_2] < [VO\{OC(NH_2)_2\}_2Cl_2] < [VOCl_4]^{2-}$ for the vanadyl halide systems. Each trend parallels the increase in the V–Cl bond length (see Fig. 1). For the NCS^- complexes, the thiocyanate charge of −0.639 for $[VO(NCS)_4]^{2-}$ increases by 0.049 to −0.688 for $[VO(NCS)_4(OH_2)]^{2-}$ despite the slightly shorter V–N contact in the latter. This result might be consistent with arguments based on Pauling's electroneutrality principle which would suggest that the donation from the water ligand would lead to a general reduction in donation from the other ligands. However, the charge on the water changes by only 0.046 on co-ordination while that on the vanadyl oxygen has decreased, despite a longer V=O contact. The combined effects of the vanadyl and water oxygens appear to be sufficient to increase the total charge on the thiocyanates. For $[VO(CN)_5]^{3-}$ the lower charge on the equatorial cyanides simply reflects the shorter bond length.

The spin populations demonstrate that delocalisation occurs predominantly *via* spin polarisation. This is expected since the unpaired electron resides in a π-type orbital not heavily involved in covalent bonding. The main polarisation is located in the vanadyl unit with a large negative spin population of −0.20 to −0.26 appearing on the oxygen atom. This generally results in a positive spin population on the metal of about 1.2. For the chloride-containing species and for $[VO(CN)_5]^{3-}$, spin transfers to the ligands are generally negative but quite small while for $[VO(NCS)_4]^{2-}$, $[VO(NCS)_4(OH_2)]^{2-}$ and to a lesser degree, $[VO\{OC(NH_2)_2\}_2Cl_2]$ some of the excess spin on the metal appears as positive spin density on the ligands.

The total charge and spin densities allow for some comparison between the complexes, but these quantities are not wholly satisfactory. For example, the NCS^- ligand is expected to be a stronger donor than, say, Cl^- yet for all the vanadyl chloro species more charge is removed from the chlorides than from the thiocyanates, at least relative to the isolated ions. A better way of comparing disparate ligands is through the overlap population (Table 10) Again, the V–Cl overlap populations vary according to bond length, *viz.* $VCl_4 > [VCl_5]^-(Cl_{eq}) > [VCl_5]^-(Cl_{ax})$, with bond lengths of 2.10, 2.172 and 2.300 Å respectively and $[VO(NMe_3)_2Cl_2] > [VO\{OC(NH_2)_2\}_2Cl_2] > [VOCl_4]^{2-}$, with bond lengths of 2.25, 2.34 and 2.42 Å respectively.

A comparison between $[VOCl_4]^{2-}$ and $[VO(NCS)_4]^{2-}$ indicates that the V–NCS bond is indeed stronger than the V–Cl bond. However, for the mixed-ligand species $[VO\{OC(NH_2)_2\}_2Cl_2]$ and $[VO(NMe_3)_2Cl_2]$ the V–Cl bond length shortens progressively; so much so that in $[VO(NMe_3)_2Cl_2]$ the V–Cl overlap of 0.500 now exceeds the V–N value of 0.465 in $[VO(NCS)_4]^{2-}$. The $V-CN_{eq}$ overlap is the largest of any of the vanadyl complexes, consistent with the highly covalent V–CN bonding. Interestingly, the $V-CN_{eq}$ overlap is similar to the V–Cl value in VCl_4 which has the shortest V–Cl bond.

The large overlap populations for the vanadyl V–O bond are consistent with considerable covalent bonding. About one third of the total arises from σ-symmetry overlap with two thirds from π overlap. There is obviously a strong multiple V–O bond. The detailed variation of the total V–O overlap seems to correlate quite well with the V–O distance with the exception of the V–O contact in $[VO(NMe_3)_2Cl_2]$. This bond is shorter than in both $[VO\{OC(NH_2)_2\}_2Cl_2]$ and $[VO(CN)_5]^{3-}$ and yet $[VO(NMe_3)_2Cl_2]$ has the smallest V–O overlap. Many attempts have been made to correlate the V–O bond length (and hence bond strength) with the nature of the basal ligands but it has recently been concluded[3] 'that there is no safe generalisation to be made'. Taking only the five-co-ordinate complexes, the V–O overlaps vary in the order $[VO(NCS)_4]^{2-} > [VOCl_4]^{2-} > [VO\{OC(NH_2)_2\}_2Cl_2] > [VO(NMe_3)_2Cl_2]$ while the average magnitude of the equatorial ligand overlaps varies as $[VO(NCS)_4]^{2-} > [VO(NMe_3)_2Cl_2] > [VO\{OC(NH_2)_2\}_2Cl_2] > [VOCl_4]^{2-}$ These two series suggest, for $[VO(NCS)_4]^{2-}$ at least, that an increase in the equatorial

Table 11 Calculated and experimental d–d transition energies (cm^{-1}). All theoretical values are computed *via* the transition-state procedure. Literature assignments are indicated in parentheses

Complex	Method	ΔE_1	ΔE_2	ΔE_3	ΔE_4	Ref.
VCl_4	DVMPOL	8 471				
	Exptl.	9 000				53
$[VCl_5]^-$	DVMPOL	131	5 762	7 211	18 413	
	Exptl	—	6 200	8 100	16 000	54
$[VOCl_4]^{2-}$	DVMPOL	12 100(I)	13 281(II)	22 159(III)		
	Exptl.	11 600(I)	13 700(II)	21 400(III)		2
$[VO(NCS)_4]^{2-}$	DVMPOL	13 625(II)	20 807(I)	21 326(III)		
	Exptl.	14 060(II)	17 720(I)	22 400(III)		2
$[VO(NCS)_4(H_2O)]^{2-}$	DVMPOL	13 958(II)	14 207(II)	22 179(I)	26 239(III)	
	Exptl.	13 300	13 300	17 400(I)	>26 000(III)	2
$[VO(CN)_5]^{3-}$	DVMPOL	15 244(II)	29 537(I)	35 458(III)		
	Exptl.	15 000(II)	25 400(I)	>30 000(III)		2
$[VO\{OC(NH_2)_2\}_2Cl_2]$	DVMPOL	13 677(I)	13 288(II)	13 592(II)	22 113(III)	
	Exptl.	12 570(I)	14 280(II)	14 280(II)	21 943(III)	2
$[VO(NMe_3)_2Cl_2]$	DVMPOL	10 760	13 009	17 478	26 169	
	Exptl.	11 760	13 150	14 200	27 030	5

ligand donation actually enhances the V–O overlap rather than weakening it as conventional wisdom anticipates.[3] Evidently, Money *et al.*[3] are correct in that the complexities of the bonding in vanadyl complexes cannot be simply rationalised.

For the six-co-ordinate species, the aqua ligand plays a very minor role in the geometry and electronic structure of $[VO(NCS)_4(OH_2)]^{2-}$, while the axial CN^- ligand in $[VO(CN)_5]^{3-}$ exerts a profound influence on the V–O bond length which, at 1.642 Å, it is the longest of any complex studied here. Overall, it seems that the bonding in each complex must be dealt with individually and that attempts to predict the properties of one complex from those of other apparently related species may be ill advised.

d–d Spectra.—One of the main aims of this work is to extend the DVXα treatment of the electronic spectra of d^1 systems from $[CrOCl_4]^-$ to V^{IV} and vanadyl complexes. Near-quantitative reproduction of the d–d and c.t. bands in $[CrOCl_4]^-$ was obtained[20] using Slater's transition state (t.s.) formalism.[38] Complete (DVMPOL) t.s. calculations of the d–d spectra for all the complexes studied here are compared with experimental data in Table 11. Any reported assignments of these bands for the vanadyl complexes are included following the usual convention of labelling bands I, II and III as the one-electron promotions $d_{xy} \longrightarrow d_{x^2-y^2}$, $d_{xy} \longrightarrow d_{xz}$, d_{yz} and $d_{xy} \longrightarrow d_{z^2}$ respectively. Overall, the agreement between the DVXα results and the experimental band maxima is excellent. In all cases bar $[VO(CN)_5]^{3-}$ there are three bands calculated to lie below 30 000 cm^{-1}. The average error is only about 10% except for band I of the NCS and CN complexes which is overestimated by between 15 and 20%.

The DVXα treatment of VCl_4 yields excellent agreement with experiment.[53] No assignment of the spectrum of $[VCl_5]^-$ accompanied the experimental measurements so the calculation seeks only to reproduce the reported band energies.[54] Overall, experiment is reproduced to within about 10% which is quite satisfactory. The numerical agreement is even more impressive for $[VOCl_4]^{2-}$ due in part to the detailed choice of geometry. The computed sequence of d–d band energies is I < II < III. This is the first calculation on $[VOCl_4]^{2-}$ to achieve the same assignment as that derived unambiguously from detailed single-crystal data.[2] Previous theoretical studies have invariably predicted the reverse order of bands I and II. The latter assignment happens to agree with the original Ballhausen–Gray (BG) scheme[7] but is contrary to the spectroscopic data in this case. The MSXα treatment of $[VOCl_4]^{2-}$[14] also gave the BG assignment which can be traced to the choice of molecular geometry. The authors report band I and band II energies of 12 950 and 9220 cm^{-1} respectively. Using their geometry, DVXα SCC t.s. calculations yield values of 11 467 and 9522 cm^{-1}.

Of course, the BG scheme was developed from a treatment of the $[VO(OH_2)_5]^{2+}$ ion rather than $[VOCl_4]^{2-}$. It was recognised[7] that the relative ordering of bands I and II would depend on the equatorial ligand field and may well change with different donors. The increased strength of the V–NCS bonding in $[VO(NCS)_4]^{2-}$ re-established band II at lower energy than band I. The DVXα results again give reasonably good numerical agreement with experiment,[2] but perhaps more importantly, the assignment of the d–d bands is correctly predicted. The presence of an axial water in $[VO(NCS)_4(OH_2)]^{2-}$ would be expected to increase the band III energy without changing the other two maxima unduly. The computed band III energy for $[VO(NCS)_4(OH_2)]^{2-}$ does indeed increase by 5000 cm^{-1} relative to $[VO(NCS)_4]^{2-}$ with band I increasing by some 1400 cm^{-1} in agreement with this prediction. The observation[2] of essentially two peaks, band II at about 13 300 cm^{-1} and band I at 17 400 cm^{-1}, is supported by the DVXα calculations. Band III is calculated to fall above 26 000 cm^{-1} where it is presumably obscured by more intense c.t. absorption.

Band III for $[VO(CN)_5]^{3-}$ is computed to lie well above 30 000 cm^{-1} and is not observed. Band II agrees well with experiment[2] but band I is again calculated several thousand wavenumbers too high. It could be argued for the NCS complexes that since the structural data do not pertain to *exactly* the same compounds as those used to obtain the spectroscopic data[2] there may be small errors in the geometries. Such errors may lead to a discrepancy in the band I energies. This argument does not hold for $[VO(CN)_5]^{3-}$ where all the experimental data pertain to $K_3[VO(CN)_5]$. It therefore appears that the relatively poorer treatment of the band I transition is inherent in the computational procedure. The method can, of course, be further improved by increasing the basis set size and/or using higher multipoles in the fitting of the Coulomb potential but there seems little to be gained from further computations in this instance.

The final two systems, $[VO\{OC(NH_2)_2\}Cl_2]$ and $[VO(NMe_3)_2Cl_2]$ not only extend the DVXα treatment to other ligands but also demonstrate the model's ability to handle much larger molecules. Extensive fine structure is observed[2] for the urea complex leading to a relatively unambiguous assignment. Only three bands are located in the single-crystal spectra despite the rhombic symmetry of the complex. This indicates (*a*) that the fourth band apparently observed[12] in the solution spectra of $[VO\{OC(NH_2)_2\}_2Cl_2]$ is spurious and (*b*) that the effective spectroscopic symmetry is close to C_{4v}. The DVXα calculations do indeed predict a splitting of only 304 cm^{-1} between the components of band II as opposed to a value of 1750 cm^{-1} from

the EHMO treatment.[12] However, the present results also place bands I and II in the reverse order to experiment.[2] Since the overall splitting between the computed transitions is so small, this is not a a significant error.

Another interesting feature of the DVXα results for $[VO\{OC(NH_2)_2\}_2Cl_2]$ concerns the ground-state orbital sequence compared to the t.s. results. In the ground state there are two ligand-based levels *below* the mainly d_{z^2} function. However, t.s. calculations for these orbitals place them, as expected, *above* band III at 28 808 and 30 100 cm^{-1} respectively. The relaxation accompanying what are essentially M→L c.t. transitions is very much larger than for the d–d transitions. The numerical agreement between experimental and DVXα d–d band maxima is thus again very good for $[VO\{OC(NH_2)_2\}_2Cl_2]$ and appears to give a generally more accurate and reliable description of the electronic structure and bonding than does the EHMO method.

No polarised single-crystal spectra of $[VO(NMe_3)_2Cl_2]$ appear to be available. The reported assignment of the d–d bands is based on chemical arguments and intensities derived from the dubious technique of Gaussian analysis.[5] No particular significance is attached to this assignment therefore. The calculated transition energies (Table 11) show good agreement with experiment apart from the third band which is estimated some 3300 cm^{-1} higher than observed. This transition corresponds to the $d_{xy} \longrightarrow d_{xz}$ promotion and is heavily influenced by the V–Cl σ interaction. The V–Cl bond in $[VO(NMe_3)_2Cl_2]$ is very short and a slight overestimation of the V–Cl interaction may well be responsible for the high energy of the third transition. Overall, however, the data in Table 11 show once again the near-quantitative accuracy of the DVXα method.

Electron Spin Resonance Spectra.—A calculation of the ESR g and A values for $[VOCl_4]^{2-}$ is included for illustrative purposes using previously reported expressions.[14] The values were computed from the DVMPOL treatment of $[VOCl_4]^{2-}$. The basis-set calculation gave a value of $\langle r_{3d}^{-3} \rangle$ of 2.7196 au^{-3} yielding $P = 127.44 \times 10^{-4}$ cm^{-1}. The Fermi contact term was then computed to be 0.735 using $A_0 = -98 \times 10^{-4}$ cm^{-1} and $g_0 = 1.9687$. Associating the partial charges from the Mulliken analysis with the squares of the appropriate MO coefficients gives the following values for the ESR parameters (the experimental values from ref. 14 follow in parentheses): $g_{\|} = 1.9371$ (1.948), $g_{\perp} = 1.9734$ (1.979), $|A_{\|}| = 167.9 \times 10^{-4}$ cm^{-1} (168.8×10^{-4} cm^{-1}) and $|A_{\perp}|$ 63.8×10^{-4} cm^{-1} (62.8×10^{-4} cm^{-1}). Both hyperfine constants are computed to be less than zero. The experimental observation of $g_{\|} < g_{\perp}$ is predicted and there is good numerical agreement all round.

Conclusion

DVXα DVMPOL calculations on the d^1 vanadium(IV) complexes VCl_4 and $[VCl_5]^-$ together with the six vanadyl molecules $[VOCl_4]^{2-}$, $[VO(NCS)_4]^{2-}$ $[VO(NCS)_4(OH_2)]^{2-}$, $[VO(CN)_5]^{3-}$, $[VO\{OC(NH_2)_2\}_2Cl_2]$ and $[VO(NMe_3)_2Cl_2]$ yield near-quantitative reproduction of the d–d band maxima and, equally importantly, their assignments. Significantly, this high level of accuracy applies to simple molecules, like VCl_4, as well as to more complicated systems, like $[VO(NMe_3)_2Cl_2]$. The fast, efficient DVXα approach gives accurate results for complete molecules rather than truncated model species. Moreover, the inherent one-electron density functional formalism leads to a straightforward commentary on the nature of the metal–ligand bonding based on charges and overlap populations. The bonding in the vanadyl species displays a complex interaction between the VO^{2+} unit and the other ligands. Simple correlations between bond lengths and overlap populations are not obvious. However, the present success of the DVXα model indicates that predictions based on accurate calculations should be reliable. This result has important consequences for modelling the electronic structures of transition-metal complexes. The growing confidence in the high quality of the DVXα scheme suggests that the study of the spectroscopic properties of biologically important metal species will be fruitful.

References

1 J. Selbin, *Chem. Rev.*, 1965, **65**, 163; *Coord. Chem. Rev.*, 1966, **1**, 293.
2 D. Collison, B. Gahan, C. D. Garner and F. E. Mabbs, *J. Chem. Soc., Dalton Trans.*, 1980, 667.
3 J. K. Money, J. C. Huffman and G. Cristou, *Inorg. Chem.*, 1985, **24**, 3297.
4 P. A. Kilty and D. Nicholls, *J. Chem. Soc. A*, 1966, 1175.
5 J. E. Drake, J. Vekris and J. S. Wood, *J. Chem. Soc. A*, 1968, 1000.
6 R. A. D. Wentworth and T. S. Piper, *J. Chem. Phys.*, 1964, **41**, 3884.
7 C. J. Ballhausen and H. B. Gray, *Inorg. Chem.*, 1962, **1**, 111.
8 L. G. Vanquickenborne and S. P. McGlynn, *Theor. Chim. Acta*, 1968, **9**, 390.
9 M. Zerner and M. Gouterman, *Inorg. Chem.*, 1966, **5**, 1699.
10 J. E. Drake, J. Vekris and J. S. Wood, *J. Chem. Soc A*, 1969, 345.
11 H. J. Stoklosa, J. R. Wasson and B. J. McCormick, *Inorg. Chem.*, 1974, **13**, 592.
12 H. A. Kuska and P. H. Yang, *Inorg. Chem.*, 1974, **13**, 1090.
13 K. K. Sunil and M. T. Rogers, *Inorg. Chem.*, 1981, **20**, 3283.
14 K. K. Sunil, J. F. Harrison and M. T. Rogers, *J. Chem. Phys.*, 1982, **76**, 3087.
15 P. Amoros, R. Ibanez, A. Beltran and D. Beltran, *J. Chem. Soc., Dalton Trans.*, 1988, 1665.
16 J. R. Winter and H. B. Gray, *Comments Inorg. Chem.*, 1981, **1**, 4.
17 C. D. Garner, J. Kendrick, P. Lambert, F. E. Mabbs and I. H. Hillier, *Inorg. Chem.*, 1976, **15**, 1287.
18 J. Weber and C. D. Garner, *Inorg. Chem.*, 1980, **19**, 2206.
19 D. Collison, *J. Chem. Soc., Dalton Trans.*, 1989, 1.
20 R. J. Deeth, *J. Chem. Soc., Dalton Trans.*, 1990, 365.
21 R. J. Deeth, *J. Chem. Soc., Dalton Trans.*, 1990, 355.
22 H. Adachi, S. Shiokawa, M. Tsukada, C. Satoko and S. Sugano, *J. Phys. Soc. Jpn.*, 1979, **47**, 1528.
23 E. J. Baerends, D. E. Ellis and P. Ros, *Theor. Chim. Acta*, 1972, **27**, 339.
24 M. Sano, H. Adachi and H. Yamatera, *Bull. Chem. Soc. Jpn.*, 1981, **54**, 2898.
25 G. S. Chandler, R. J. Deeth, B. N. Figgis and R. A. Phillips, *J. Chem. Soc., Dalton Trans.*, 1990, 1417.
26 E. J. Baerends and P. Ros, *Mol. Phys.*, 1975, **30**, 1735.
27 R. M. Kowaleski, F. Basolo, J. H. Osborne and W. C. Trogler, *Organometallics*, 1988, **7**, 1425.
28 L. Verluis, T. Ziegler, E. J. Baerends and W. Ravenek, *J. Am. Chem. Soc.*, 1989, **111**, 2018.
29 H. Adachi, M. Tsukada and C. Satoko, *J. Phys. Soc. Jpn.*, 1978, **45**, 875.
30 W. C. Trogler, D. E. Ellis and J. Berkowitz, *J. Am. Chem. Soc.*, 1979, **101**, 5896.
31 G. F. Holland, D. E. Ellis and W. C. Trogler, *J. Am. Chem. Soc.*, 1986, **108**, 1884.
32 R. J. Deeth, B. N. Figgis and M. I. Ogden, *Chem. Phys.*, 1988, **121**, 115.
33 A. Rosen, D. E. Ellis, H. Adachi and F. W. Averill, *J. Chem. Phys.*, 1976, **65**, 3629.
34 B. Delley and D. E. Ellis, *J. Chem. Phys.*, 1982, **76**, 1949.
35 F. W. Averill and D. E. Ellis, *J. Chem. Phys.*, 1973, **59**, 6412.
36 E. J. Baerends, D. E. Ellis and P. Ros, *Chem. Phys.*, 1973, **2**, 41.
37 R. S. Mulliken, *J. Chem. Phys.*, 1955, **23**, 1833, 1841.
38 J. C. Slater, *Quantum Theory of Molecules and Solids*, McGraw-Hill, New York, 1974, vol. 4.
39 W. Haase and H. Hopper, *Acta Crystallogr., Sect. B*, 1968, **24**, 282.
40 L. O. Atovmyan and Z. G. Aliev, *Zh. Strukt. Khim.*, 1970, **11**, 782.
41 B. Gahan, C. D. Garner, L. H. Hill, F. E. Mabbs, K. D. Hargrave and A. T. McPhail, *J. Chem. Soc., Dalton Trans.*, 1977, 1726.
42 W. N. Lipscomb and A. G. Whittaker, *J. Am. Chem. Soc.*, 1945, **67**, 2019.
43 V. P. Spiridonov and G. V. Ramanov, *Zh. Strukt. Khim.*, 1967, **8**, 160.
44 M. L. Ziegler, B. Nuber, K. Weidenhammer and G. Hoch, *Z. Naturforsch., Teil B*, 1977, **32**, 18.
45 K. Zhou, Y. Xu and J. Huang, *J. Struct. Chem.*, 1984, **3**, 61.
46 S. Jagner and N. Vannenberg, *Acta Chem. Scand.*, 1973, **27**, 3482.
47 J. Coetzel, *Acta Crystallogr., Sect. B*, 1970, **26**, 872.

48 C. A. L. Becker and J. P. Dahl, *Theor. Chim. Acta*, 1970, **19**, 135.
49 D. A. Copeland and C. J. Ballhausen, *Theor. Chim. Acta*, 1971, **20**, 317.
50 T. Parameswaran and D. E. Ellis, *J. Chem. Phys.*, 1973, **38**, 2088.
51 C. W. G. Russell and D. W. Smith, *Inorg. Chim. Acta*, 1972, **6**, 677.
52 R. J. Deeth, Ph.D. Dissertation, Cambridge University, 1985.
53 F. A. Blankenship and R. L. Belford, *J. Chem. Phys.*, 1962, **36**, 633.
54 I. M. Griffiths, D. Nicholls and K. R. Seddon, *J. Chem. Soc A*, 1971, 2513.

Received 22*nd October* 1990; *Paper* 0/04739B